
NEW ALLOMETRIC MODELS FOR THE USA CREATE A STEP-CHANGE IN FOREST CARBON ESTIMATION, MODELING, AND MAPPING

A PREPRINT

Lucas K Johnson 

Division of Environmental Science
State University of New York College of Environmental Science and Forestry
Syracuse, NY, 13210
ljohns11@esf.edu

Michael J Mahoney 

Division of Environmental Science
State University of New York College of Environmental Science and Forestry
Syracuse, NY, 13210
mjmahone@esf.edu

Grant M Domke 

Northern Research Station
USDA Forest Service
St. Paul, MN, 55108
grant.m.domke@usda.gov

Colin M Beier 

Department of Sustainable Resources Management
State University of New York College of Environmental Science and Forestry
Syracuse, NY, 13210
cbeier@esf.edu

2024-05-07

ABSTRACT

The United States national forest inventory (NFI) serves as the foundation for forest aboveground biomass (AGB) and carbon accounting across the nation. These data enable design-based estimates of forest carbon stocks and stock-changes at state and regional levels, but also serve as inputs to model-based approaches for characterizing forest carbon stocks and stock-changes at finer spatial and temporal resolutions. Although NFI tree and plot-level data are often treated as truth in these models, they are in fact estimates based on regional species-group models and parameters known collectively as the Component Ratio Method (CRM). In late 2023 the Forest Inventory and Analysis (FIA) program introduced a new National Scale Volume and Biomass Estimators (NSVB) system to replace CRM nationwide and offer more precise and accurate representations of forest AGB and carbon. Given the prevalence of model-based AGB studies relying on FIA, there is concern about the transferability of methods from CRM to NSVB models, as well as the comparability of existing CRM AGB products (e.g. maps) to new and forthcoming NSVB AGB products. To begin addressing these concerns we compared previously published CRM AGB maps and estimates to new maps and estimates produced using identical methods with NSVB AGB reference data. Our

results suggest that models relying on passive satellite imagery (e.g. Landsat) provide acceptable estimates of point-in-time NSVB AGB and carbon stocks, but fail to accurately quantify growth in mature closed-canopy forests. We highlight that existing estimates, models, and maps based on FIA reference data are no longer compatible with NSVB, and recommend new methods as well as updated models and maps for accommodating this step-change. Our collective ability to adopt NSVB in our modeling and mapping workflows will help us provide the most accurate spatial forest carbon data possible in order to better inform local management and decision making.

Keywords aboveground biomass • national forest inventory • Landsat • design-based estimation • model-based estimation

1 Introduction

Measuring and monitoring forest biomass is an active area of research, with mapped predictions of forest aboveground biomass (AGB) in particular being used to inform carbon accounting efforts alongside other conservation and stewardship activities. In the US context, such maps often rely upon AGB estimates from the US Forest Inventory and Analysis program (FIA) which provides tree-level AGB estimates for millions of trees across thousands of plots throughout the US (Gray et al. 2012). These tree-level estimates can then be aggregated to plots and used to estimate AGB across the landscape (Bechtold and Patterson 2005). However, these design-based estimates are limited to a relatively coarse spatial resolution due to the density of the FIA sample (McRoberts 2011). A plethora of studies have demonstrated using model-based estimation to produce AGB estimates at finer resolutions, fitting models to predict FIA's AGB estimates using remote sensing data products (for instance, Kennedy, Ohmann, et al. 2018; Johnson et al. 2022, 2023; Huang et al. 2019; Ayrey et al. 2021; Zheng, Heath, and Ducey 2007). These studies commonly treat the AGB estimates provided by FIA as ground truth and adopt them with only minimal adjustments or corrections (if any).

However, FIA's AGB estimates are not actual ground truth measurements, but are instead calculated by applying allometric models to quantities more easily measured in the field. Historically these estimates have been calculated using the component ratio method (CRM, Woodall, Heath, et al. 2011; Heath et al. 2009), a combination of regional species-group-specific allometric models that estimate biomass as a function of tree diameter and height. Although AGB estimates from CRM are useful, they do have several limitations. In particular, CRM models for non-merchantable portions of trees were not constructed using actual tree component measurements and the administrative boundaries used to delineate regional models did not correspond to underlying ecological gradients.

In light of these limitations and the rapidly growing interest in measuring and monitoring AGB and forest carbon stocks, FIA introduced a new National Scale Volume and Biomass Estimators (NSVB) system to replace CRM nationwide in late 2023 (Westfall et al. 2023). NSVB estimates of AGB address the primary concerns with CRM and provide a more unified and accurate set of estimates for AGB across the nation. NSVB also represents a step-change in forest AGB estimation, with NSVB estimating 14.6% more forest AGB nationwide than CRM estimates using the same field measurements. This difference varies across geographic regions and forest compositions with differences in estimated state-level AGB ranging from +37.1% for Indiana to -1.5% for Washington (Westfall et al. 2023; Virginia Tech 2023a, 2023c). A major driver of these differences appears to be improvements to the estimation of top and limb biomass, and as a result species that are poor self-pruners or otherwise grow denser tops and branches often (though not always) saw the largest increases in estimated AGB under NSVB.

The new AGB and carbon estimates introduced with NSVB do not reflect on-the-ground changes in forest structure or function, but simply represent accounting changes resulting from swapping one system of allometric models for another. Although they are purely structural, these accounting changes aim to improve our understanding of forest AGB and carbon stocks and fluxes across the landscape by increasing the precision and accuracy of tree-level volume, biomass, and carbon estimates. Therefore it is necessary to update existing carbon-monitoring systems that rely on FIA estimates of AGB or carbon to incorporate the benefits of NSVB in resulting map products and estimates. However, given the importance of top and limb biomass in NSVB estimates, it is not clear if common model-based approaches relying on remotely sensed data (which may have difficulty penetrating the canopy to capture the density of tops and branches in a forest) will be effective at predicting NSVB estimates. This in turn has obvious downstream implications for how forest carbon accounting will be impacted by the shift from CRM to NSVB estimates of forest AGB and carbon stocks, and suggests the urgent need to revisit existing modeling pipelines holistically rather than exchanging individual components (e.g. reference data sets) in isolation. Further, there exists concern about the comparability of existing maps produced using CRM AGB to newer products produced using NSVB AGB. It is not yet known whether AGB maps produced using NSVB will be simple “rescalings” of their CRM equivalents, or if these new maps will exhibit new patterns across focal landscapes. These questions and concerns are particularly pressing given the proliferation of AGB models based on FIA data and both the growing demand and technical capacity for remote monitoring of forest carbon stocks.

To begin answering these questions, we compared previously published AGB maps fit using CRM AGB estimates to new maps produced using identical methods and NSVB AGB estimates. Specifically, we 1) replicated the methodology of Johnson et al. (2023), a well-established empirical modeling approach relying on field inventory plots and Landsat imagery (Lu 2006; Hall et al. 2006; Powell et al. 2010; Pflugmacher, Cohen, and E. Kennedy 2012; Deo et al. 2016; Kennedy, Ohmann, et al. 2018), to produce maps of AGB based on NSVB. 2) We compared these new NSVB-based AGB maps against CRM-based maps from Johnson et al. (2023) for 2005 and 2019. 3) We then quantified the agreement between these maps, the differences in their AGB stock-change estimates for 2005-2019, the spatial patterns of these differences, and the ability for machine learning models fit using Landsat imagery to estimate CRM and NSVB AGB overall.

2 Methods

2.1 Study area

New York State covers 141,297 km² of the northeastern United States. Daily temperatures across the state ranged from -17 °C to 28 °C in 2019, while monthly precipitation for the same period ranged from 5.0 cm to 16.8 cm (NOAA National Centers for Environmental Information 2022). Elevation ranges from -2 m to 1,584 m above sea level (U.S. Geological Survey 2019). The majority of the state occupies the northern hardwoods-hemlock forest region, though there are important inclusions of beech-maple-basswood and Appalachian oak communities in the western and southern reaches of the state, respectively (Dyer 2006). Like much of the US Northeast, NYS was extensively deforested during the 18th and 19th centuries, with subsequent reforestation and conservation resulting in a landscape dominated by forest stands that are now over 100 years old (Whitney 1994; Lorimer 2001; Mahoney et al. 2022). NYS created the Forest Preserve in 1885, establishing the foundation for what became the Adirondack and Catskill Parks decades later. Any state-owned or acquired lands within these parks has since been designated as ‘forever wild’ and has largely been preserved, with no timber harvesting.

The US Forest Service estimates that NSVB-induced changes to AGB estimates for New York State will be moderate, with an estimated 5.7% increase in AGB statewide (Virginia Tech 2023b). This increase is not distributed evenly across species, however; FIA estimates that red spruce (*Picea rubens*) AGB will increase by approximately 38.7%, while sugar maple (*Acer saccharum*) AGB will increase by just under 5%, and yellow birch (*Betula alleghaniensis*) AGB will decrease by roughly 5% (Virginia Tech 2023b). These species are not uniformly distributed throughout the state: red spruce is most common in high-elevation forests throughout the Adirondack Park, sugar maple is the largest contributor to statewide total standing biomass (Virginia Tech 2023b) with highest abundance in montane regions with more mature forests, often in combination with yellow birch (Wilson, Lister, and Riemann 2012; Riemann et al. 2014). As a result, it is not yet known how local to regional estimates of forest AGB and carbon sequestration will be impacted by the shift to NSVB.

2.2 Modeling NSVB AGB

We repeated the methods used in the “direct” modeling procedure from Johnson et al. (2023) to develop AGB maps for New York State using NSVB AGB estimates and Landsat imagery from 2005 and 2019 as summarized below.

2.2.1 Field inventory data

Each FIA plot contains four 7.32 m radius (24 ft) circular subplots, one at the center of the plot and three centered 36.6 m (120 ft) away from the plot center at azimuths of 120°, 240°, and 360° (Bechtold and Patterson 2005). We obtained true plot centroids for FIA plots within New York State under an agreement with the FIA program office. Plots are assigned to one of five panels, each assumed to have complete spatial coverage across the state, and remeasured on a 5-7 year basis. Trees on land considered to be forested within each subplot above 12.7 cm (5 in) DBH are measured and assigned AGB estimates. We aggregated tree-level AGB estimates to the FIA plot-level, and area-normalized these estimates to convert them into units of Mg ha⁻¹. FIA considers land to be forested if an area at least 0.4 ha in size and 120m in width is not developed for nonforest land uses and is at least 10% stocked with trees. Under this definition, it is likely that some woody AGB exists on some of these nonforest lands not measured by FIA. However, in the absence of field measurements for these areas, we treated these nonforest lands as having 0 AGB.

We filtered the complete set of FIA plots within New York State measured between 2002 and 2019 to only those inventories where all four subplots were measured. When plots in this filtered set were inventoried multiple times, we randomly selected a single inventory year to avoid pseudoreplication. This initial selection criteria resulted in a pool of 5,144 plots. We then divided this set of plots into model development and map assessment datasets using FIA’s panel designation, with one of the five panels randomly selected and all plots with this designation assigned to the map assessment dataset, and the remaining plots assigned to the model development dataset. In this way we partitioned 20% of the available data for an independent map assessment, yielding a probability sample with complete spatial coverage

which allowed us to use design-unbiased estimators for map agreement metrics (Riemann et al. 2010; Stehman and Foody 2019).

We then filtered the model development set to only include completely forested (and therefore completely measured) plots. We then added to this set a group of completely nonforested plots with maximum LiDAR-derived canopy heights $\leq 1\text{m}$, which we assumed to correspond to having 0 AGB (Johnson et al. 2022), resulting in a total of 2,049 model development plots. The map assessment set was further filtered to remove plots external to our mapped area based on our landcover mask (Johnson et al. 2023), as these plots were outside our population of interest, resulting in 545 assessment plots.

2.2.2 Auxiliary data

Following Mahoney et al. (2022), we derived a set of 16 predictors from annual growing-season medoid composites of Landsat collection 1 imagery (USGS 2018) using coefficients from Roy et al. (2016). These predictors were then processed using Landtrends in Google Earth Engine using normalized burn ratio temporally segmented vertices to produce a smoothed continuous 30-year time series of pixel-level metrics (Kennedy, Yang, and Cohen 2010; Kennedy, Yang, et al. 2018). Metrics derived included normalized burn ratio (Kauth and Thomas 1976), tasseled-cap wetness, brightness, and greenness (Cocke, Fulé, and Crouse 2005), normalized difference vegetation index (Kriegler et al. 1969), simple ratio (Jordan 1969), and modified simple ratio (Chen 1996), as well as the one-year change at each pixel for each of these indices. Index calculation used the spectral module for Google Earth Engine (Montero et al. 2022). We additionally calculated the years since the most recent disturbance from the normalized burn ratio segmentation, with a temporal range from 1985-2019, and the associated magnitude of change in normalized burn ratio.

To this set of auxiliary data we added annual primary and secondary land cover classifications from the US Geological Survey's Land Change Monitoring, Assessment and Projection (LCMAP) version 1.2 (Zhu and Woodcock 2014; Brown et al. 2020) and a set of steady-state variables including 30 year normals for precipitation and temperature (PRISM Climate Group 2022), elevation, aspect, slope, and topographic wetness index derived from a 30 m digital elevation model (Beven and Kirkby 1979; U.S. Geological Survey 2019; Mahoney, Beier, and Ackerman 2022), estimates from a 2005 global canopy height model (Simard et al. 2011; Hudak et al. 2020), distance to nearest waterbodies identified by the US Census Bureau (US Census Bureau 2013; Walker 2023), National Wetland Inventory classifications from the US Fish and Wildlife Service, and the Environmental Protection Agency's level 4 ecozones (Omernik and Griffith 2014; CEC 1997). Ecozones were aggregated to their corresponding level 3 ecozone if they did not cover $\geq 2\%$ of the state. If the aggregated level 3 ecozones also did not cover $\geq 2\%$ of the state, they were assigned an ecozone of "other".

All auxiliary data was projected to match Landsat 30 m pixel geometries, using the terra package (Hijmans 2023) for the R programming language (R Core Team 2023). We used the exactextractr library to associate the gridded auxiliary data with FIA plots (described in Section 2.2.1), calculating the mean of pixel values intersecting with subplot locations weighted by the fraction of each pixel overlapping with the plot area (Baston 2022).

2.2.3 Model fitting

We further partitioned the model development data set (described in Section 2.2.1) into a training set (80% of observations) and a testing set (20% of observations). We fit a random forest as implemented in the ranger R package (Breiman 2001; Wright and Ziegler 2017), a gradient boosting machine as implemented in the lightgbm R package (Friedman 2002; Ke et al. 2017; Shi et al. 2022), and a support vector machine as implemented in the kernlab R package (Cortes and Vapnik 1995; Karatzoglou et al. 2004) to this training set. Hyperparameters were selected for each method through an iterative grid search using five-fold cross-validation. More information on this tuning procedure is available in Section 2.6 (Model development) of Johnson et al. (2023).

We then used five-fold cross-validation to generate predictions from each of these models, using their selected hyperparameters, for each observation in the training data set. We then fit a linear regression estimating plot AGB as a function of these predictions, ensembling the three base models in order to produce a single final prediction (Wolpert 1992; Dormann et al. 2018). We selected this ensemble model as our final model; all further discussions of model accuracy and predictions refer to this ensemble. Following Johnson et al. (2023), and in order to avoid redundant comparisons between models of NSVB and CRM AGB, we focused only on the map accuracy assessment and have provided model testing set metrics in Supplementary Materials A.

2.3 Mapping and postprocessing

We used the ensemble model to make predictions for all 30 m pixels across the state for both 2019, the most recent map year in Johnson et al. (2023), and 2005, the earliest year possible to produce a statewide design-based estimate from the public FIA database. Following Johnson et al. (2023), we masked our predictions with annual LCMAP version 1.2 primary landcover classification product to remove developed, cropland, water, and barren pixels. We then compared these maps to CRM-based maps representing 2019 and 2005 from Johnson et al. (2023).

2.4 Map accuracy assessment

As this study represents one of the first (if not the first) model-based estimation studies based on NSVB AGB, we perform a comprehensive map accuracy assessment of our NSVB AGB model following methods described in Riemann et al. (2010). Using the ensemble model, we predicted AGB at each 30m pixel coincident with FIA plots, using predictors derived from Landsat imagery from the same year as the FIA inventory. We then used the exactextractr library to calculate the mean of these pixel predictions at each plot, weighted by the fraction of each pixel overlapping with the plot area (Baston 2022).

Following Riemann et al. (2010) we calculated model assessment metrics both directly using these weighted averages and FIA plot-level estimates (plot-to-pixel) and after aggregating predictions and FIA plot-level estimates to multiple regular grids of variably-sized hexagons, increasing in size such that hexagon centroids ranged from 2 km to 50 km apart (1 km separation yields the equivalent to a plot-to-pixel comparison).

Model assessment metrics included root-mean squared error (RMSE; Equation 1), mean absolute error (MAE; Equation 2), mean error (ME; Equation 3), and R^2 (Equation 4):

$$\text{RMSE} = \sqrt{\left(\frac{1}{n}\right) \sum_{i=1}^n (y_i - \hat{y}_i)^2} \quad (1)$$

$$\text{MAE} = \left(\frac{1}{n}\right) \sum_{i=1}^n |y_i - \hat{y}_i| \quad (2)$$

$$\text{ME} = \left(\frac{1}{n}\right) \sum_{i=1}^n y_i - \hat{y}_i \quad (3)$$

$$R^2 = 1 - \frac{\sum_{i=1}^n (y_i - \hat{y}_i)^2}{\sum_{i=1}^n (y_i - \bar{y})^2} \quad (4)$$

Where y_i is FIA estimated AGB, \hat{y}_i is model-predicted AGB, and \bar{y} is mean FIA estimated AGB.

Interpreting RMSE and MAE can be difficult, as these metrics are in units of Mg ha^{-1} which can make interpret the relative magnitude of errors challenging without also knowing the mean and distribution of pixel AGB values. To aid interpretation, we present normalized variants of these metrics rescaled by the mean AGB within the training data set:

$$\text{RMSE \%} = 100 \cdot \frac{\text{RMSE}}{\bar{y}} \quad (5)$$

$$\text{MAE \%} = 100 \cdot \frac{\text{MAE}}{\bar{y}} \quad (6)$$

These metrics are well-suited to describing a single model, or for comparing multiple models fit to the same data set. However, they are not well suited for comparing models fit to outcomes pulled from different distributions. In order to compare the performance of models fit to NSVB AGB estimates to the CRM AGB model from Johnson et al. (2023), we instead used the dimensionless d_r statistic from Willmott, Robeson, and Matsuura (2011):

$$d_r = \left\{ \begin{array}{l} 1 - \frac{\sum_{i=1}^n |\hat{y}_i - y_i|}{c \sum_{i=1}^n |y_i - \bar{y}|}, \text{ when} \\ \sum_{i=1}^n |\hat{y}_i - y_i| \leq c \sum_{i=1}^n |y_i - \bar{y}| \\ \frac{c \sum_{i=1}^n |y_i - \bar{y}|}{\sum_{i=1}^n |\hat{y}_i - y_i|} - 1 \text{ otherwise} \end{array} \right\} \quad (7)$$

The d_r metric is bounded $[-1, 1]$, with a value of 1 indicating perfect agreement between y and \hat{y} . It is an asymmetrical metric which assumes that y are ‘‘true’’ values, which is appropriate for comparing model predictions to FIA estimates.

As such, we calculated d_r for both the model fit using NSVB AGB and the model fit using CRM AGB, using the corresponding set of FIA AGB estimates, in order to compare how well these models represent FIA AGB estimates.

Each of these metrics was calculated at a plot-to-pixel scale and after aggregation to each grid of hexagons. Metric calculations used the waywiser R package (Mahoney 2023).

Finally, using the same set of map assessment plots, we assessed how well the distribution of predictions from CRM and NSVB AGB models approximated the distributions of their corresponding FIA estimates using empirical cumulative distribution function plots and Kolmogorov-Smirnov (KS) tests (Massey Jr 1951).

2.5 Map comparisons

We directly compared a 2019 NSVB AGB map produced in this study to a 2019 CRM AGB map produced by the direct modeling approach in Johnson et al. (2023) through raster differencing. We differenced AGB maps and percent rank maps to identify spatial patterns of both absolute changes between CRM and NSVB predictions as well as shifts relative to the statewide distributions. We also assessed the agreement between these 2019 AGB maps across multiple scales of aggregation with variably-sized hexagons (centroids 1 km to 50 km apart; Section 2.4; Riemann et al. (2010)) using the agreement coefficient (AC; Equation 8) from Ji and Gallo (2006):

$$AC = 1 - \frac{\sum_{i=1}^n (\hat{y}_i - y_i)^2}{\sum_{i=1}^n (|\hat{y} - \bar{y}| + |\hat{y}_i - \hat{y}|) (|\hat{y} - \bar{y}| + |y_i - \bar{y}|)} \quad (8)$$

Here y represents predictions from the CRM model, while \hat{y} represents predictions from the NSVB model. AC is a symmetrical metric which allows for errors in both y and \hat{y} , making it useful to compare model predictions to one another. AC is bounded $[-\infty, 1]$, with a value of 1 representing perfect agreement.

A benefit of AC is that it can be broken down into systematic and unsystematic components by first estimating a geometric mean functional relationship (GMFR) model (Equation 9) to predict y as a function of \hat{y} (Draper and Yang 1997):

$$\begin{aligned} y' &= a + b\hat{y} \\ b &= \pm \left(\frac{\sum_{i=1}^n (\hat{y}_i - \bar{\hat{y}})^2}{\sum_{i=1}^n (y_i - \bar{y})^2} \right)^{\frac{1}{2}} \\ a &= \bar{\hat{y}} - b\bar{y} \end{aligned} \quad (9)$$

Where the sign of b is the same as the correlation coefficient between y and \hat{y} , and y' represents GMFR-predicted values of y .

We then use the GMFR to predict \hat{y} as a function of y , which we term \hat{y}' :

$$\hat{y}' = -\frac{a}{b} + \frac{1}{by} \quad (10)$$

We then use \hat{y}' to decompose the sum of squared differences in the numerator of AC (Equation 8), into its unsystematic (AC_u , Equation 11) and systematic (AC_s , Equation 12) components:

$$AC_u = 1 - \frac{\sum_{i=1}^n [(|\hat{y}_i - \hat{y}'_i|) (|y_i - y'_i|)]}{\sum_{i=1}^n (|\hat{y} - \bar{y}| + |\hat{y}_i - \hat{y}|) (|\hat{y} - \bar{y}| + |y_i - \bar{y}|)} \quad (11)$$

$$AC_s = 1 - \frac{\left(\sum_{i=1}^n (\hat{y}_i - y_i)^2 \right) - \left(\sum_{i=1}^n [(|\hat{y}_i - \hat{y}'_i|) (|y_i - y'_i|)] \right)}{\sum_{i=1}^n (|\hat{y} - \bar{y}| + |\hat{y}_i - \hat{y}|) (|\hat{y} - \bar{y}| + |y_i - \bar{y}|)} \quad (12)$$

In this way, we were able to determine the degree to which differences in maps produced using CRM AGB are systematically different from maps produced using NSVB AGB, and therefore the degree to which they could be linearly rescaled to match NSVB-based estimates. Further details of this derivation are provided in Ji and Gallo (2006).

We tested rescaling model-based CRM AGB to model-based NSVB AGB with a simple linear regression as follows:

Table 1: NSVB AGB map accuracy results (vs FIA) for select scales. RMSE, MAE, ME in Mg ha^{-1} . Scale = distance between hexagon centroids in km; PPH = plots per hexagon; n = number of comparison units (plots or hexagons). All metrics as defined in Section 2.3.

Scale	n	PPH	MAE	% MAE	RMSE	% RMSE	ME	R ²	d _r
Plot:Pixel	545		47.25	36.01	60.33	45.97	-3.86	0.37	0.60
20 km	293	1.86	39.82	30.03	52.66	39.72	-2.32	0.39	0.61
30 km	171	3.19	35.85	26.99	48.28	36.34	-0.72	0.39	0.62
50 km	74	7.38	28.24	20.93	38.87	28.81	3.39	0.44	0.63

$$\text{NSVB}_{\text{mod}} = \beta_0 + \beta_1 \cdot \text{CRM}_{\text{mod}} + \beta_2 \cdot \text{Elevation} \quad (13)$$

Where NSVB_{mod} , CRM_{mod} , and *Elevation* were pixel-level values sampled from a raster stack containing maps of NSVB and CRM AGB (2019; Mg ha^{-1}) and elevation (m) as layers. We randomly divided the 1,000,000 pixel sample into training (80%; n = 800,000) and testing (20%; n = 200,000) sets for model fitting and assessment respectively.

2.6 Statewide stock estimates

We additionally compared estimates of statewide AGB stocks calculated across both sets of estimation methods (design-based vs model-based approaches) and allometric models (CRM vs NSVB). We estimated total NYS AGB and aboveground carbon (AGC) stocks for 2005 and 2019 using design-based estimates following methods described in Pugh et al. (2018), using FIA inventory data with both NSVB and CRM-based AGB estimates. These estimates included stems 12.7 cm (5 inches) and up and correspond to all land in NYS. We then calculated model-based AGB stocks for both the CRM and NSVB-based models by multiplying the average pixel-level AGB density (Mg ha^{-1}) by the total area of NYS. Following CRM protocols described in Woodall, Heath, et al. (2011), AGC stocks were assumed to be 50% of AGB for all model-based CRM estimates. Under the new NSVB protocols described in Westfall et al. (2023), species-specific carbon fractions are used to convert AGB to AGC. We did not have access to a fine-resolution species map for NYS in our map years, but instead computed statewide carbon fractions for each respective map-year (2005 and 2019) as an average of species-specific carbon fractions, weighted by each species' relative contribution to FIA's statewide AGB estimates. We used these fractions to convert model-based estimates of statewide total NSVB AGB to statewide total NSVB AGC.

2.7 Comparing stock-changes with NSVB and CRM

We computed statewide design-based and Landsat-based stock-change estimates by subtracting the 2005 estimates for each method from their corresponding 2019 estimates. Additionally, we compared pixel-level stock-changes by first computing stock change maps as 2019 AGB minus 2005 AGB for NSVB and CRM and then differencing these stock change maps ($\Delta \text{NSVB} - \Delta \text{CRM}$). We used this stock-change difference map to identify landscape patterns of differences in statewide stock-change estimates.

3 Results

3.1 NSVB Map Accuracy

Mapped AGB predictions from the NSVB model became increasingly accurate and exhibited higher agreement with FIA estimates as aggregation unit size increased, with % MAE decreasing from 36.01 to 20.93%, % RMSE decreasing from 45.97 to 28.81%, R² increasing from 0.37 to 0.44, and d_r increasing from 0.60 to 0.63 (Table 1; Figure 1). RMSE and MAE followed similar patterns. ME estimates were small across all scales of assessment and did not exhibit a monotonic improvement with aggregation (Table 1).

3.2 NSVB vs CRM Map

Both NSVB and CRM maps (Figure 2) yielded similar agreement with corresponding FIA estimates across all scales of aggregation; the dimensionless d_r statistics (ranging from -1 to 1) differed by at most 0.02 between the approaches (Figure 3). CRM and NSVB AGB models approximated the distributions of their corresponding FIA estimates similarly (Figure 4), but NSVB models appeared to be more impacted by saturation, a common issue when modeling forest structure with passive satellite imagery (Lu 2005; Duncanson, Niemann, and Wulder 2010; Johnson et al. 2023), where models underpredict the largest reference observations. Kolmogorov-Smirnov statistics confirmed that CRM AGB models were only marginally better at approximating the corresponding FIA distribution (CRM 0.17; NSVB 0.18).

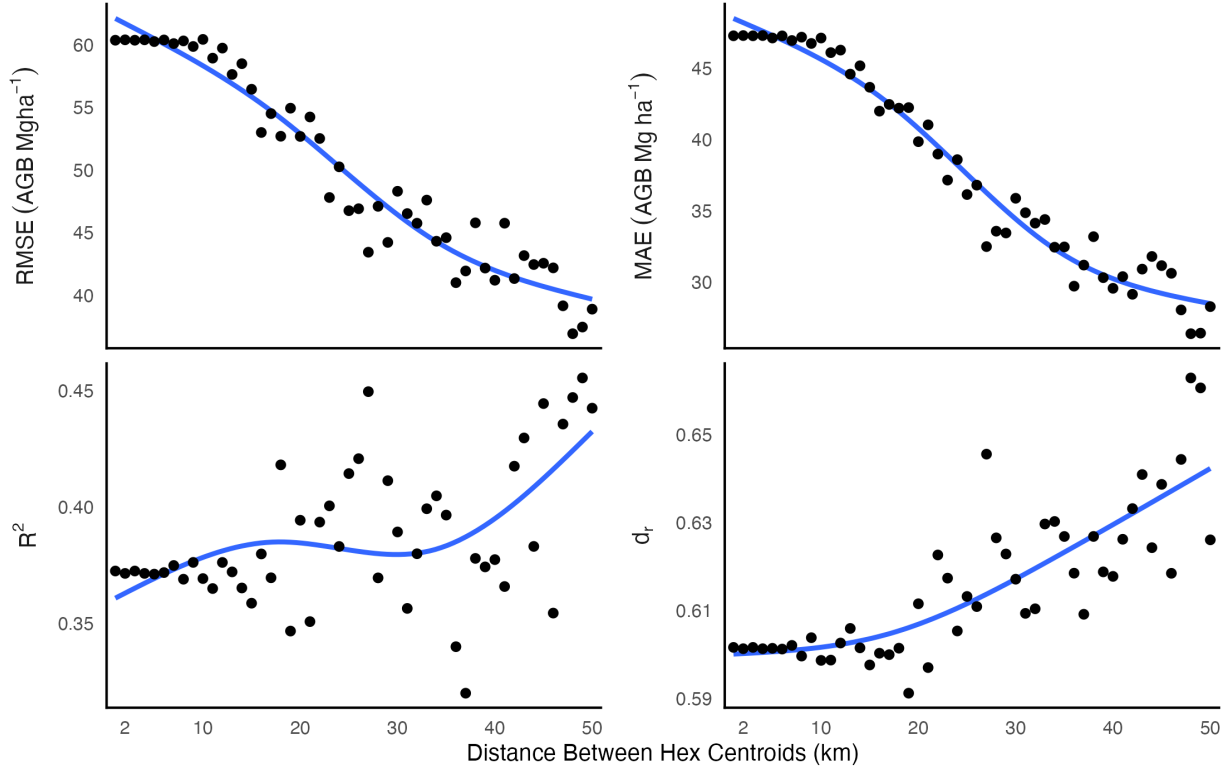


Figure 1: NSVB AGB map accuracy results (vs FIA) across multiple scales represented by distances between hexagon centroids. Blue lines are fit to data using cubic splines with three knots.

Table 2: Results of a regression model representing model-based NSVB AGB (Mg ha^{-1}) as a function of model-based CRM AGB (Mg ha^{-1}) and elevation (m).

	Coefficient	Standard error	t	p
Intercept	9.555	0.050	189.855	< 0.001
CRM AGB	1.135	< 0.001	3,322.265	< 0.001
Elevation	-0.023	< 0.001	-275.981	< 0.001

NSVB and CRM AGB maps agreed well with one another across all scales of aggregation ($AC > 0.9$), but agreement worsened with increasing aggregation (Figure 5). The majority of the disagreement was due to systematic differences between the maps (ACs). The AGB difference map showed that models of NSVB AGB produced larger estimates relative to models of CRM AGB across most of NYS, but produced smaller estimates concentrated in what appear to be the montane forests of the Adirondack and Catskill regions (Figure 6 a). In contrast to the AGB difference map, the percent rank difference map showed a more uniform pattern of downshifts and upshifts in percent rank across NYS, highlighting ‘gaining’ and ‘losing’ areas in terms of AGB density (more or less AGB relative to the rest of the state) with a shift to NSVB. High-elevation areas still contained the largest relative downshifts in percent rank from CRM to NSVB (Figure 6 b) indicating that models estimated these areas to be much less AGB-dense relative to the rest of NYS following a change from CRM to NSVB.

The linear regression (Equation 13) used to rescale CRM AGB to NSVB AGB was accurate (RMSE 14.05, MAE 10.91, ME -0.01) and represented 93% (R^2) of the variability in the model-based NSVB predictions from the test set. The regression coefficients succinctly described the observed spatial patterns of differences between model-based CRM and NSVB AGB (Figure 6), indicating that NSVB AGB would increase by $\sim 1.14 \text{ Mg ha}^{-1}$ with every unit increase in CRM AGB and elevation held constant, but that NSVB AGB would decrease by $\sim 2 \text{ Mg ha}^{-1}$ for every 100 m of elevation gained and CRM AGB held constant (Table 2; Supplementary Materials B).

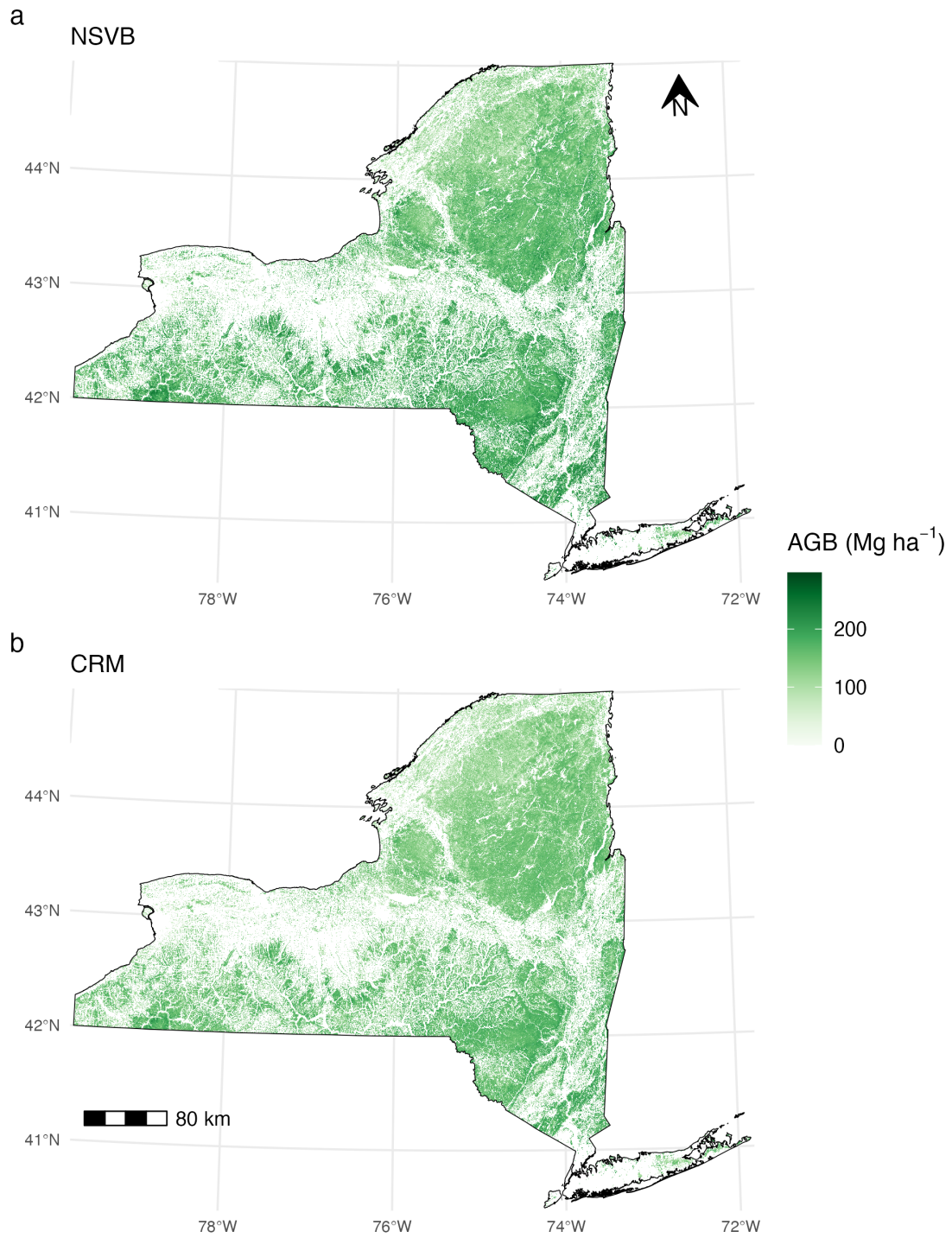


Figure 2: Landsat modeled AGB for 2019. a) Predictions made with models trained on NSVB-based FIA reference data. b) Predictions made with models trained on CRM-based FIA reference data.

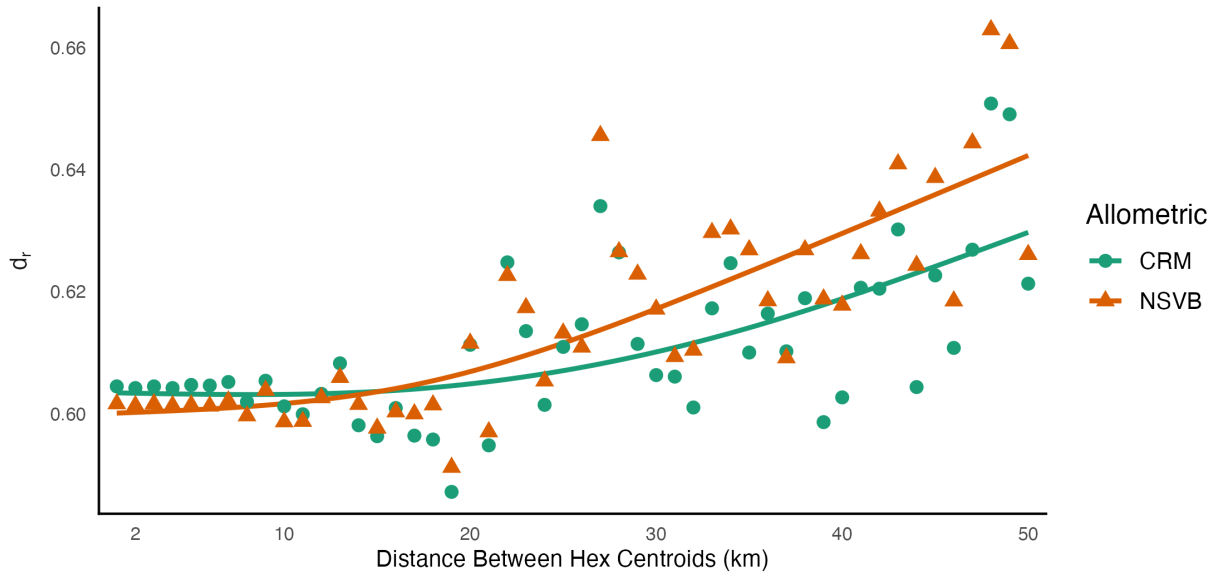


Figure 3: Willmott’s d_r (measure of agreement, 1 is perfect; Section 2.4) across scales represented by distances between hexagon centroids. Landsat-based NSVB AGB vs FIA-based NSVB AGB (orange) and Landsat-based CRM AGB vs FIA-based CRM AGB (green). Trend lines fit to data using cubic splines with three knots.

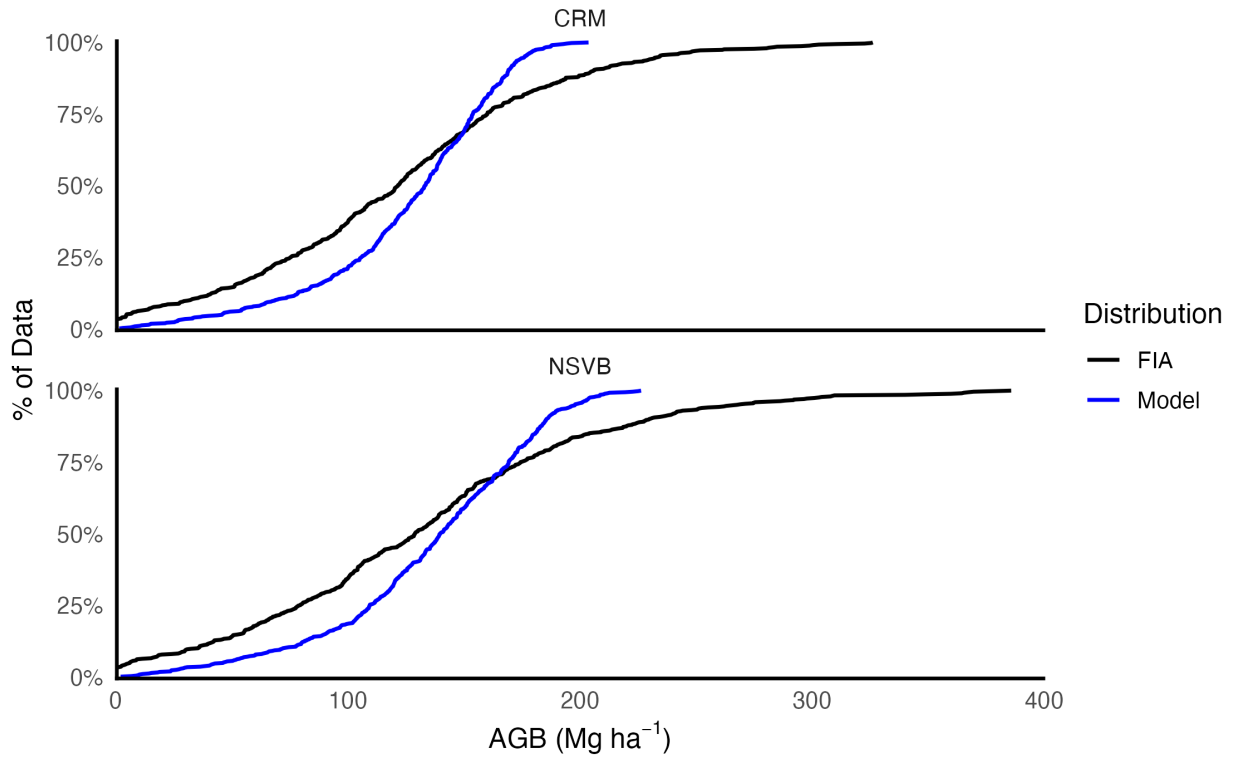


Figure 4: Empirical cumulative distribution function comparisons. Landsat-modeled predictions of AGB vs FIA plot-level estimates of AGB for NSVB and CRM respectively.

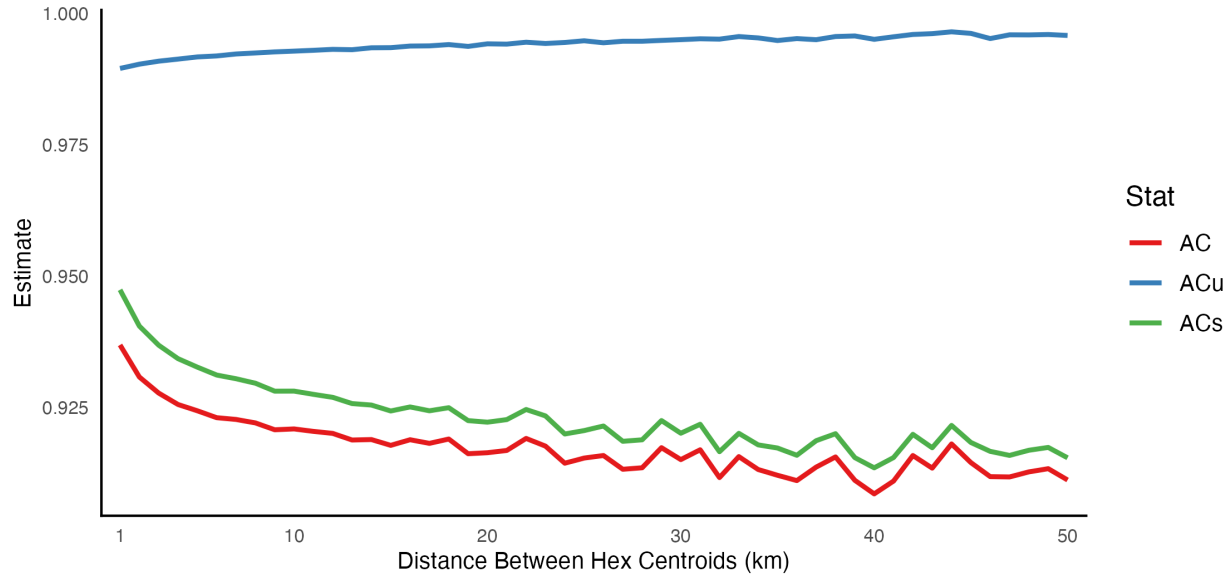


Figure 5: Agreement between NSVB AGB maps and CRM AGB maps across scales represented by distances between hexagon centroids. AC (agreement coefficient) and its systematic (ACs) and unsystematic (ACu) components as defined in Section 2.5.

Table 3: Statewide stocks (2019, 2005) and stock-changes (Δ ; 2019 minus 2005) for aboveground biomass (AGB) and aboveground carbon (AGC) by estimation method (FIA vs Landsat) and allometric (CRM vs NSVB). Values in millions of metric tons.

		CRM			NSVB		
		FIA	Landsat	FIA - Landsat	FIA	Landsat	FIA - Landsat
AGB	2005	910.29	943.01	-32.72	967.42	1106.10	-138.68
	2019	1038.87	1063.90	-25.03	1129.59	1213.03	-83.44
	Δ	128.58	120.90	7.68	162.17	106.93	55.24
AGC	2005	455.14	471.50	-16.36	467.89	534.87	-66.98
	2019	519.44	531.95	-12.51	546.13	586.69	-40.56
	Δ	64.29	60.45	3.84	78.24	51.81	26.43

3.3 Stock and stock-change comparison

Estimates of total NSVB AGB and AGC for NYS were substantially larger than corresponding CRM estimates for both the design-based and model-based methods (Table 3). However, while design-based stock-change estimates were greater when using NSVB allometrics, model-based stock-change estimates using NSVB were smaller than their CRM counterparts. Additionally, there was greater divergence between design-based and model-based estimates of both statewide AGB and AGC when using NSVB instead of CRM (Table 3).

The model-based stock-change maps for NSVB and CRM yielded nearly identical spatial distributions of AGB losses and gains, however the magnitudes of losses and gains differed (Figure 7 a, b). AGB losses from 2005 to 2019 appeared to be greater in magnitude in the NSVB map than in the corresponding CRM map, particularly in the Adirondack region in the northeastern portion of the state (Figure 7 c). NSVB AGB gains over the time period were only marginally larger than corresponding CRM AGB gains throughout the south-central region, and along the southeastern border of the state.

4 Discussion

In this study we investigated the transferability of well-established methods for estimating, modeling, and mapping aboveground biomass (AGB) based on Landsat imagery between two USDA Forest Inventory and Analysis (FIA) reference data sets constructed with different systems of allometric models: the legacy Component Ratio Method (CRM, Woodall, Domke, et al. 2011) and the new National Scale Volume and Biomass Estimators (NSVB, Westfall et al.

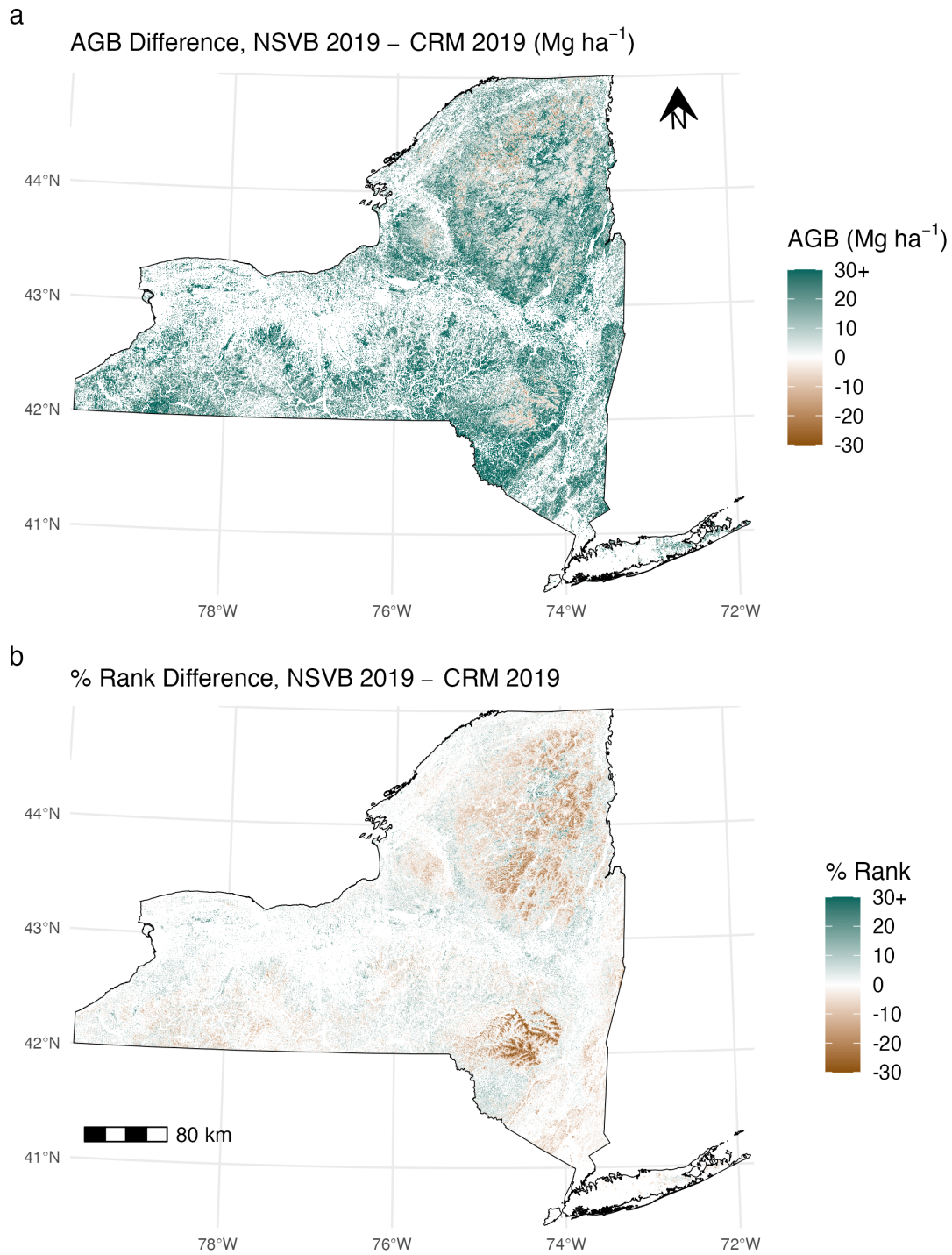


Figure 6: Difference maps for 2019 computed as Landsat-modeled AGB with NSVB-based FIA reference data minus Landsat-modeled AGB with CRM-based FIA reference data. a) AGB differences in units of Mg ha^{-1} b) Percent rank differences. Mapped values capped at ± 30 .

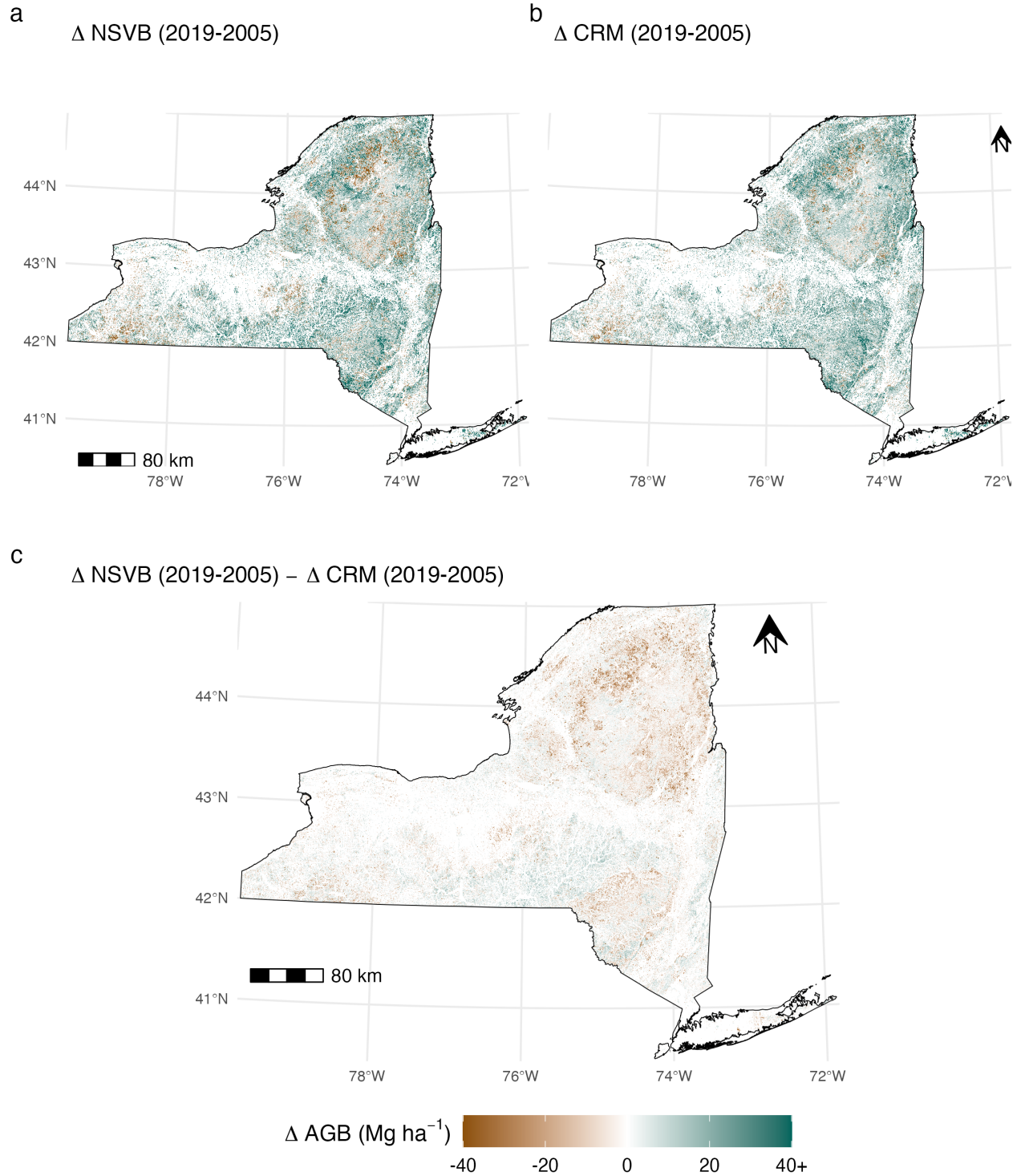


Figure 7: Stock-change map comparison. a) 15-year NSVB stock-change map (Δ NSVB; 2019 AGB - 2005 AGB). b) 15-year CRM stock-change map (Δ CRM; 2019 AGB - 2005 AGB). c) Stock-change difference map computed as Δ NSVB minus Δ CRM. Mapped values capped at $\pm 40 \text{ Mg ha}^{-1}$.

2023). To this end, we compared previously published CRM AGB maps and derived estimates (Johnson et al. 2023) to new maps and derived estimates produced using identical methods but with NSVB AGB reference data. We found that NSVB and CRM AGB maps agreed well with one another, though systematic differences driven by NSVB allometric equations were apparent in our maps; NSVB AGB predictions were generally larger than corresponding CRM AGB predictions and concentrations of smaller NSVB AGB existed in high-elevation regions of the state. Maps of NSVB and CRM AGB agreed similarly with corresponding FIA reference data sets, however models of NSVB AGB were more impacted by saturation and thus were limited in their ability to characterize AGB growth beyond a certain point. These findings demonstrate that NSVB represents a step-change for model-based forest carbon estimation and monitoring in the United States (US) and suggest the need to update entire modeling pipelines, especially for applications that require the representation of forest growth over time. In particular incorporating NSVB-based reference data in carbon monitoring systems may require updated models, careful comparisons with CRM-based estimates, and new modeling approaches including additional remotely sensed datasets such as LiDAR.

4.1 Comparing NSVB and CRM AGB maps

We interpreted that the differences between our NSVB and CRM AGB maps (Figure 6) were driven by changes in the underlying system of allometric models, specifically how CRM and NSVB estimates differed for individual species and size classes. NSVB was designed (in part) to yield more precise estimates of top and limb biomass and as a result, the majority of the differences between the estimates from the two systems can be attributed to these non-merchantable components of trees (Westfall et al. 2023; Virginia Tech 2023b). Within NYS, an FIA estimated 57.5% increase in statewide top and limb biomass contributed to an overall 5.7% increase in total AGB (Virginia Tech 2023b). This increase was generally reflected in our map differences where NSVB AGB model predictions were larger than corresponding CRM AGB predictions across most of the state. NSVB AGB increases relative to CRM AGB may be most pronounced for large-diameter individuals and for species that are poor self-pruners or otherwise grow densely-packed branches (Westfall et al. 2023; Virginia Tech 2023b). Conversely, trees in high-elevation areas where we observed smaller predictions of NSVB AGB relative to CRM AGB (Table 2; Figure 6) often have smaller stems due to shallow soils and more frequent windthrow and ice storms. Thus, it stands to reason that high-elevation forests generally would not see the same increase in top and branch biomass with the transition to NSVB as more size- and species-diverse forests throughout the state. These same montane regions contain large proportions of sugar maple and yellow birch (Wilson, Lister, and Riemann 2012; Riemann et al. 2014) which were among the species that did not show large AGB increases associated with the transition to NSVB (Virginia Tech 2023b). These map differences exemplify the degree to which updates and improvements to allometric models may yield structural changes to downstream model-based estimates along relevant ecological gradients such as species composition, climate, and topography.

Although there were notable differences between maps (Figure 6), statistical comparisons indicated a high degree of agreement between NSVB and CRM AGB maps (Figure 5). Agreement (AC, ACs) decreased as a function of aggregation unit size, indicating that differences were spatially clustered (particularly in the aforementioned high-elevation forests), and thus were amplified through aggregation. Across all scales of aggregation, most of the disagreement between mapped predictions was attributed to systematic differences, due to the relatively uniform increase in AGB under NSVB in most forested regions of the state. As a result, it was possible to translate existing CRM AGB estimates to their NSVB equivalents through relatively simple linear relationships (Table 2; Equation 13). However, any such adjustments outside the scope of this study will require further investigation, will likely be model- and task-specific, and should be performed with care given the spatial variability of NSVB-CRM differences.

4.2 Difficulty modeling NSVB AGB growth with passive remote sensing

While the relative increase in FIA-estimated stocks from CRM to NSVB were mirrored with model-based estimates, the relative decrease in model-based estimates of stock-changes from CRM to NSVB contradicted design-based estimates which showed greater stock-changes under NSVB (Table 3). This significantly widened the gap between design- and model-based stock-change estimates from 7.68 million metric tons of AGB under CRM, to 55.24 million metric tons of AGB when using NSVB, calling into question the ability of Landsat-based models to quantify NSVB stock-changes and forest growth. The introduction of species-specific carbon fractions with NSVB appeared to have minimal impact on aboveground carbon estimates relative to the impact of differences in AGB.

We did find that NSVB AGB models fit using Landsat imagery were still able to generate acceptable point-in-time AGB stock estimates as evidenced by the comparable agreement with FIA-reference plots in our map accuracy assessment (Figure 3). Further, this study does not cast doubt on the ability of NSVB AGB models to detect discrete canopy changes driven by deforestation, reforestation, and disturbance events. However, under NSVB, a greater number of plots had AGB values beyond the saturation point for model predictions, indicating that models of NSVB AGB were less capable of accurately estimating AGB in denser forest stands with larger individual trees than models of CRM AGB (Figure 4). This may be caused by the increased precision and magnitude of NSVB biomass estimates for the tops and

limbs of trees (Westfall et al. 2023), particularly for larger-diameter trees. These components are difficult to “see from space”, particularly in forests with closed canopies where this biomass is largely hidden from passive satellite imagery.

Our results therefore suggest that passive remote sensing alone may not be capable of monitoring NSVB AGB growth, especially in regions similar to NYS and the much of the Northeastern US where historical land-use dynamics indicate that the majority of forest stands have either reached or are approaching maturity (Section 2.1). The inclusion of active remote sensing systems in NSVB modeling pipelines, including aerial and spaceborne LiDAR or synthetic aperture radar, may offer the only solutions to monitoring NSVB AGB growth at scale, as these classes of sensors have the capacity to penetrate closed canopies and better represent structural attributes related to AGB, thus reducing saturation effects (Quegan et al. 2019; Dubayah et al. 2020; Johnson et al. 2022). Using repeat aerial LiDAR collections to estimate NSVB AGB growth would be a first step in this direction.

4.3 Implications for carbon accounting

FIA plot data has been widely used as reference data in model-based approaches to forest carbon accounting in the US (e.g. Kennedy, Ohmann, et al. 2018; Johnson et al. 2022, 2023; Huang et al. 2019; Ayrey et al. 2021; Zheng, Heath, and Ducey 2007). Given the reported changes associated with NSVB (Westfall et al. 2023), it is perhaps unsurprising that our results show significant differences between model-based NSVB AGB maps and estimates and their CRM counterparts. However, we have revealed the potential spatial variability of differences within a state, uncovered challenges with model-based monitoring of NSVB AGB over time, and have confirmed the role of species and size-classes in creating regions of forest carbon gains and losses under a shift to NSVB. In light of these challenges, the spatial distribution of differences, and the general lack of consensus on accounting protocols among carbon markets, there may be incentives to act in bad faith. Of particular concern is the opportunity to deliberately choose one system over another on a case-by-case basis in order to maximize payments or credits for avoided deforestation, afforestation, or improved management (Gillenwater et al. 2007; Charnley, Diaz, and Gosnell 2010; Kaarakka et al. 2021). We therefore underscore that this step-change represents an advance towards a more realistic representation of forest carbon density across the landscape and thus should be adopted as quickly as possible. Rescaling existing model-based estimates of CRM AGB to NSVB equivalents (Equation 13; Table 2) may serve as a temporary solution to understand how estimates will change or how decisions may have been different under NSVB. However, it is crucial that models and maps of CRM AGB are retrained and updated to make the NSVB transition, especially if we aspire towards map products that have the most possible practical relevance for local management and carbon accounting.

Another factor to consider in the NSVB transition is the accurate conversion of biomass to carbon stocks. NSVB introduced species-specific carbon fractions, offering improved AGC accuracy over the 0.5 AGB to AGC ratio assumed with CRM, but at the cost of increased complexity. Under CRM it was standard practice to map AGB and simply convert these initial pixel-level predictions to AGC or belowground carbon (BGC) using fractions that applied to all species (Woodall, Heath, et al. 2011; Heath et al. 2009). We followed this standard approach in this study for the sake of comparison to AGB maps produced in Johnson et al. (2023) and only converted our estimates to AGC for estimates of statewide totals using a species-weighted carbon fraction (Section 2.6). However, under NSVB this AGB-first approach carries the additional requirement of species maps with matching resolution, extent, and general timestamp in order to correctly convert each pixel prediction (Riemann et al. 2014; Wilson, Lister, and Riemann 2012; Wilson et al. 2013). Alternatively, practitioners may opt to model AGC (or BGC) directly, choosing to incorporate species-specific carbon fractions into reference data at the plot-level. Stand maps, or regional species-group maps, may provide a middle road where pixel-level AGB predictions could be aggregated to stands or regions with approximately known species compositions, and more targeted species-weighted carbon ratios could be applied as we did here for statewide estimates of AGC.

5 Conclusion

This study represents a first-of-its-kind investigation into using the new National Scale Volume and Biomass Estimators (NSVB) from the USDA Forest Inventory and Analysis (FIA) program with existing model-based approaches to map forest aboveground biomass (AGB) and carbon. Our results suggest that models relying on passive satellite imagery alone (e.g. Landsat) provide acceptable estimates of point-in-time NSVB AGB and carbon stocks, but fail to appropriately quantify growth in mature closed-canopy forests. With increasing pressure for forests to sequester carbon and offset greenhouse gas emissions from other sectors, models that under-predict or mischaracterize forest growth will not serve to maximize the role forested landscapes will play in natural climate solutions and policies. We highlight that existing maps based on FIA reference data are no longer compatible with NSVB, and recommend incorporating active remote sensing data, retraining models, rethinking AGB to carbon conversions, and updating maps to accommodate this step-change. Doing so is a necessity if we want to meet the growing need for accurate spatial forest carbon data that can inform management and decision making across scales.

We can interpret the good practices for greenhouse gas inventories outlined in the 2019 refinement (Buendia et al. 2019) to the 2006 Intergovernmental Panel on Climate Change (IPCC) guidelines (Eggleston et al. 2006) as “a set of procedures intended to ensure that greenhouse gas inventories are accurate in the sense that they are systematically neither over- nor underestimates so far as can be judged, and that they are precise so far as practicable.” Thus, we have a clear obligation from the IPCC to update our GHG modeling pipelines with improved methods and data streams as they become available. However, we have demonstrated that an improvement to one component of a modeling pipeline in isolation (e.g. improved precision and accuracy in reference data) will require rethinking and retooling of other pipeline components. We therefore recommend that model pipelines be revisited holistically. This study represents one attempt at diagnosing an update involving the NSVB system of allometric models with a well-established Landsat-based modeling approach, proposes potential solutions to uncovered challenges, and identifies the overall relevance of these challenges to end-use applications such as carbon monitoring and greenhouse gas inventories.

6 Acknowledgements

We would like to thank the USDA FIA program for their data sharing and cooperation and the NYS Department of Environmental Conservation Office of Climate Change for funding support.

References

- Ayrey, Elias, Daniel J. Hayes, John B. Kilbride, Shawn Fraver, John A. Kershaw, Bruce D. Cook, and Aaron R. Weiskittel. 2021. "Synthesizing Disparate LiDAR and Satellite Datasets Through Deep Learning to Generate Wall-to-Wall Regional Inventories for the Complex, Mixed-Species Forests of the Eastern United States." *Remote Sensing* 13 (24): 5113. <https://doi.org/10.3390/rs13245113>.
- Baston, Daniel. 2022. *exactextractr: Fast Extraction from Raster Datasets Using Polygons*. <https://CRAN.R-project.org/package=exactextractr>.
- Bechtold, William A, and Paul L Patterson. 2005. *The Enhanced Forest Inventory and Analysis Program—National Sampling Design and Estimation Procedures*. Vol. 80. USDA Forest Service, Southern Research Station. <https://doi.org/10.2737/SRS-GTR-80>.
- Beven, K J, and M J Kirkby. 1979. "A Physically Based, Variable Contributing Area Model of Basin Hydrology / Un Modèle à Base Physique de Zone d'appel Variable de l'hydrologie Du Bassin Versant." *Hydrological Sciences Bulletin* 24 (1): 43–69. <https://doi.org/10.1080/02626667909491834>.
- Breiman, Leo. 2001. "Random Forests." *Machine Learning* 45 (1): 5–32. <https://doi.org/10.1023/a:1010933404324>.
- Brown, Jesslyn F., Heather J. Tollerud, Christopher P. Barber, Qiang Zhou, John L. Dwyer, James E. Vogelmann, Thomas R. Loveland, et al. 2020. "Lessons Learned Implementing an Operational Continuous United States National Land Change Monitoring Capability: The Land Change Monitoring, Assessment, and Projection (LCMAP) Approach." *Remote Sensing of Environment* 238 (March): 111356. <https://doi.org/10.1016/j.rse.2019.111356>.
- Buendia, E, K Tanabe, A Kranjc, J Baasansuren, M Fukuda, S Ngarize, A Osako, Y Pyrozhenko, P Shermanau, and S Federici. 2019. "Refinement to the 2006 IPCC Guidelines for National Greenhouse Gas Inventories." *IPCC: Geneva, Switzerland* 5: 194.
- CEC. 1997. *Ecological Regions of North America: Toward a Common Perspective*. Commission for Environmental Cooperation (Montréal, Québec).; Secretariat.
- Charnley, Susan, David Diaz, and Hannah Gosnell. 2010. "Mitigating Climate Change Through Small-Scale Forestry in the USA: Opportunities and Challenges." *Small-Scale Forestry* 9 (4): 445–62. <https://doi.org/10.1007/s11842-010-9135-x>.
- Chen, Jing M. 1996. "Evaluation of Vegetation Indices and a Modified Simple Ratio for Boreal Applications." *Canadian Journal of Remote Sensing* 22 (3): 229–42. <https://doi.org/10.1080/07038992.1996.10855178>.
- Cocke, Allison E., Peter Z. Fulé, and Joseph E. Crouse. 2005. "Comparison of Burn Severity Assessments Using Differenced Normalized Burn Ratio and Ground Data." *International Journal of Wildland Fire* 14: 189–98. <https://doi.org/10.1071/WF04010>.
- Cortes, Corinna, and Vladimir Vapnik. 1995. "Support-Vector Networks." *Machine Learning* 20 (3): 273–97. <https://doi.org/10.1007/bf00994018>.
- Deo, Ram K., Matthew B. Russell, Grant M. Domke, Christopher W. Woodall, Michael J. Falkowski, and Warren B. Cohen. 2016. "Using Landsat Time-Series and LiDAR to Inform Aboveground Forest Biomass Baselines in Northern Minnesota, USA." *Canadian Journal of Remote Sensing* 43 (1): 28–47. <https://doi.org/10.1080/07038992.2017.1259556>.
- Dormann, Carsten F., Justin M. Calabrese, Gurutzeta Guillera-Arroita, Eleni Matechou, Volker Bahn, Kamil Bartoń, Colin M. Beale, et al. 2018. "Model Averaging in Ecology: A Review of Bayesian, Information-Theoretic, and Tactical Approaches for Predictive Inference." *Ecological Monographs* 88 (4): 485–504. <https://doi.org/10.1002/ecm.1309>.
- Draper, Norman R., and Yonghong (Fred) Yang. 1997. "Generalization of the Geometric Mean Functional Relationship." *Computational Statistics & Data Analysis* 23 (3): 355–72. [https://doi.org/10.1016/s0167-9473\(96\)00037-0](https://doi.org/10.1016/s0167-9473(96)00037-0).
- Dubayah, Ralph, James Bryan Blair, Scott Goetz, Lola Fatoyinbo, Matthew Hansen, Sean Healey, Michelle Hofton, et al. 2020. "The Global Ecosystem Dynamics Investigation: High-Resolution Laser Ranging of the Earth's Forests and Topography." *Science of Remote Sensing* 1 (June): 100002. <https://doi.org/10.1016/j.srs.2020.100002>.
- Duncanson, LI, KO Niemann, and MA Wulder. 2010. "Integration of GLAS and Landsat TM Data for Aboveground Biomass Estimation." *Canadian Journal of Remote Sensing* 36 (2): 129–41. <https://doi.org/10.5589/m10-037>.
- Dyer, James M. 2006. "Revisiting the Deciduous Forests of Eastern North America." *BioScience* 56 (4): 341–52. [https://doi.org/10.1641/0006-3568\(2006\)56%5B341:RTDFOE%5D2.0.CO;2](https://doi.org/10.1641/0006-3568(2006)56%5B341:RTDFOE%5D2.0.CO;2).
- Eggleston, H S, L Buendia, K Miwa, T Ngara, and K Tanabe. 2006. "2006 IPCC Guidelines for National Greenhouse Gas Inventories."
- Friedman, Jerome H. 2002. "Stochastic Gradient Boosting." *Computational Statistics & Data Analysis* 38 (4): 367–78. [https://doi.org/10.1016/s0167-9473\(01\)00065-2](https://doi.org/10.1016/s0167-9473(01)00065-2).
- Gillenwater, Michael, Derik Broekhoff, Mark Trexler, Jasmine Hyman, and Rob Fowler. 2007. "Policing the Voluntary Carbon Market." *Nature Climate Change* 1 (711): 85–87. <https://doi.org/10.1038/climate.2007.58>.
- Gray, Andrew, Thomas Brandeis, John Shaw, William McWilliams, and Patrick Miles. 2012. "Forest Inventory and Analysis Database of the United States of America (FIA)." *Biodiversity & Ecology* 4 (September): 225–31. <https://doi.org/10.7809/b-e.00079>.

- Hall, R. J., R. S. Skakun, E. J. Arsenault, and B. S. Case. 2006. "Modeling Forest Stand Structure Attributes Using Landsat ETM+ Data: Application to Mapping of Aboveground Biomass and Stand Volume." *Forest Ecology and Management* 225 (1–3): 378–90. <https://doi.org/10.1016/j.foreco.2006.01.014>.
- Heath, L S, Mark H Hansen, James E Smith, W Brad Smith, and Patrick D Miles. 2009. "Investigation into Calculating Tree Biomass and Carbon in the FIADB Using a Biomass Expansion Factor Approach." In *2008 Forest Inventory and Analysis (FIA) Symposium*, edited by Will McWilliams, Gretchen Moisen, and Ray Czaplewski, 21–23. Fort Collins, CO: U.S. Department of Agriculture, Forest Service, Rocky Mountain Research Station; U.S. Department of Agriculture, Forest Service, Rocky Mountain Research Station.
- Hijmans, Robert J. 2023. *terra: Spatial Data Analysis*. <https://rspatial.org/>.
- Huang, Wenli, Katelyn Dolan, Anu Swatantran, Kristofer Johnson, Hao Tang, Jarlath O’Neil-Dunne, Ralph Dubayah, and George Hurtt. 2019. "High-Resolution Mapping of Aboveground Biomass for Forest Carbon Monitoring System in the Tri-State Region of Maryland, Pennsylvania and Delaware, USA." *Environmental Research Letters* 14 (9): 095002. <https://doi.org/10.1088/1748-9326/ab2917>.
- Hudak, Andrew T, Patrick A Fekety, Van R Kane, Robert E Kennedy, Steven K Filippelli, Michael J Falkowski, Wade T Tinkham, et al. 2020. "A Carbon Monitoring System for Mapping Regional, Annual Aboveground Biomass Across the Northwestern USA." *Environmental Research Letters* 15 (9): 095003. <https://doi.org/10.1088/1748-9326/ab93f9>.
- Ji, Lei, and Kevin Gallo. 2006. "An Agreement Coefficient for Image Comparison." *Photogrammetric Engineering & Remote Sensing* 72 (7): 823–33. <https://doi.org/10.14358/pers.72.7.823>.
- Johnson, Lucas K, Michael J Mahoney, Eddie Bevilacqua, Stephen V Stehman, Grant M Domke, and Colin M Beier. 2022. "Fine-Resolution Landscape-Scale Biomass Mapping Using a Spatiotemporal Patchwork of LiDAR Coverages." *International Journal of Applied Earth Observation and Geoinformation* 114 (November): 103059. <https://doi.org/10.1016/j.jag.2022.103059>.
- Johnson, Lucas K, Michael J Mahoney, Madeleine L Desrochers, and Colin M Beier. 2023. "Mapping Historical Forest Biomass for Stock-Change Assessments at Parcel to Landscape Scales." *Forest Ecology and Management* 546 (October): 121348. <https://doi.org/10.1016/j.foreco.2023.121348>.
- Jordan, Carl F. 1969. "Derivation of Leaf-Area Index from Quality of Light on the Forest Floor." *Ecology* 50 (4): 663–66. <https://doi.org/10.2307/1936256>.
- Karakka, Lilli, Meredith Cornett, Grant Domke, Todd Ontl, and Laura E. Dee. 2021. "Improved Forest Management as a Natural Climate Solution: A Review." *Ecological Solutions and Evidence* 2 (3). <https://doi.org/10.1002/2688-8319.12090>.
- Karatzoglou, Alexandros, Alex Smola, Kurt Hornik, and Achim Zeileis. 2004. "kernlab – an S4 Package for Kernel Methods in R." *Journal of Statistical Software* 11 (9): 1–20. <https://doi.org/10.18637/jss.v011.i09>.
- Kauth, Richard J., and G. S. P. Thomas. 1976. "The Tasselled Cap - a Graphic Description of the Spectral-Temporal Development of Agricultural Crops as Seen by Landsat." In *Symposium on Machine Processing of Remotely Sensed Data*, 159.
- Ke, Guolin, Qi Meng, Thomas Finley, Taifeng Wang, Wei Chen, Weidong Ma, Qiwei Ye, and Tie-Yan Liu. 2017. "LightGBM: A Highly Efficient Gradient Boosting Decision Tree." In *Advances in Neural Information Processing Systems*, edited by I. Guyon, U. V. Luxburg, S. Bengio, H. Wallach, R. Fergus, S. Vishwanathan, and R. Garnett. Vol. 30. Curran Associates, Inc. <https://proceedings.neurips.cc/paper/2017/file/6449f44a102fde848669bdd9eb6b76fa-Paper.pdf>.
- Kennedy, Robert E, Janet Ohmann, Matt Gregory, Heather Roberts, Zhiqiang Yang, David M Bell, Van Kane, et al. 2018. "An Empirical, Integrated Forest Biomass Monitoring System." *Environmental Research Letters* 13 (2): 025004. <https://doi.org/10.1088/1748-9326/aa9d9e>.
- Kennedy, Robert E, Zhiqiang Yang, and Warren B Cohen. 2010. "Detecting Trends in Forest Disturbance and Recovery Using Yearly Landsat Time Series: 1. LandTrendr — Temporal Segmentation Algorithms." *Remote Sensing of Environment* 114 (12): 2897–2910. <https://doi.org/10.1016/j.rse.2010.07.008>.
- Kennedy, Robert E, Zhiqiang Yang, Noel Gorelick, Justin Braaten, Lucas Cavalcante, Warren Cohen, and Sean Healey. 2018. "Implementation of the LandTrendr Algorithm on Google Earth Engine." *Remote Sensing* 10 (5): 691. <https://doi.org/10.3390/rs10050691>.
- Kriegler, F. J., W. A. Malila, R. F. Nalepka, and W. Richardson. 1969. "Preprocessing Transformations and Their Effects on Multispectral Recognition." In *Remote Sensing of Environment, VI*, 97.
- Lorimer, Craig G. 2001. "Historical and Ecological Roles of Disturbance in Eastern North American Forests: 9,000 Years of Change." *Wildlife Society Bulletin (1973-2006)* 29 (2): 425–39. <http://www.jstor.org/stable/3784167>.
- Lu, Dengsheng. 2005. "Aboveground Biomass Estimation Using Landsat TM Data in the Brazilian Amazon." *International Journal of Remote Sensing* 26 (12): 2509–25. <https://doi.org/10.1080/01431160500142145>.
- . 2006. "The Potential and Challenge of Remote Sensing-based Biomass Estimation." *International Journal of Remote Sensing* 27 (7): 1297–1328. <https://doi.org/10.1080/01431160500486732>.
- Mahoney, Michael J. 2023. "Waywiser: Ergonomic Methods for Assessing Spatial Models." <https://doi.org/10.48550/arXiv.2303.11312>.

- Mahoney, Michael J, Colin M Beier, and Aidan C Ackerman. 2022. “terrainr: An r Package for Creating Immersive Virtual Environments.” *Journal of Open Source Software* 7 (69): 4060. <https://doi.org/10.21105/joss.04060>.
- Mahoney, Michael J, Lucas K Johnson, Abigail Z Guinan, and Colin M Beier. 2022. “Classification and Mapping of Low-Statured Shrubland Cover Types in Post-Agricultural Landscapes of the US Northeast.” *International Journal of Remote Sensing* 43 (19-24): 7117–38. <https://doi.org/10.1080/01431161.2022.2155086>.
- Massey Jr, Frank J. 1951. “The Kolmogorov-Smirnov Test for Goodness of Fit.” *Journal of the American Statistical Association*, 68–78. <https://doi.org/10.2307/2280095>.
- McRoberts, Ronald E. 2011. “Satellite Image-Based Maps: Scientific Inference or Pretty Pictures?” *Remote Sensing of Environment* 115 (2): 715–24. <https://doi.org/10.1016/j.rse.2010.10.013>.
- Montero, D., C. Aybar, M. D. Mahecha, and S. Wieneke. 2022. “SPECTRAL: AWESOME SPECTRAL INDICES DEPLOYED VIA THE GOOGLE EARTH ENGINE JAVASCRIPT API.” *The International Archives of the Photogrammetry, Remote Sensing and Spatial Information Sciences XLVIII-4/W1-2022* (August): 301–6. <https://doi.org/10.5194/isprs-archives-xxviii-4-w1-2022-301-2022>.
- NOAA National Centers for Environmental Information. 2022. “Climate at a Glance: Statewide Mapping.” <https://www.ncdc.noaa.gov/cag/>.
- Omernik, James M., and Glenn E. Griffith. 2014. “Ecoregions of the Conterminous United States: Evolution of a Hierarchical Spatial Framework.” *Environmental Management* 54 (6): 1249–66. <https://doi.org/10.1007/s00267-014-0364-1>.
- Pflugmacher, Dirk, Warren B. Cohen, and Robert E. Kennedy. 2012. “Using Landsat-Derived Disturbance History (1972–2010) to Predict Current Forest Structure.” *Remote Sensing of Environment* 122 (July): 146–65. <https://doi.org/10.1016/j.rse.2011.09.025>.
- Powell, Scott L., Warren B. Cohen, Sean P. Healey, Robert E. Kennedy, Gretchen G. Moisen, Kenneth B. Pierce, and Janet L. Ohmann. 2010. “Quantification of Live Aboveground Forest Biomass Dynamics with Landsat Time-Series and Field Inventory Data: A Comparison of Empirical Modeling Approaches.” *Remote Sensing of Environment* 114 (5): 1053–68. <https://doi.org/10.1016/j.rse.2009.12.018>.
- PRISM Climate Group. 2022. “PRISM Climate Data.” <https://prism.oregonstate.edu>.
- Pugh, Scott A., Jeffery A. Turner, Elizabeth A. Burrill, and Winnie David. 2018. “The Forest Inventory and Analysis Database: Population Estimation User Guide.” https://www.fia.fs.usda.gov/library/database-documentation/current/ver80/FIADB%20Population%20Estimation%20user%20guide_11_2018_final_revised_02_2019.pdf.
- Qeegan, Shaun, Thuy Le Toan, Jerome Chave, Jorgen Dall, Jean-François Exbrayat, Dinh Ho Tong Minh, Mark Lomas, et al. 2019. “The European Space Agency BIOMASS Mission: Measuring Forest Above-Ground Biomass from Space.” *Remote Sensing of Environment* 227 (June): 44–60. <https://doi.org/10.1016/j.rse.2019.03.032>.
- R Core Team. 2023. *R: A Language and Environment for Statistical Computing*. Vienna, Austria: R Foundation for Statistical Computing. <https://www.R-project.org/>.
- Riemann, Rachel I., Barry T. Wilson, Andrew J. Lister, Oren Cook, and Sierra. Crane-Murdoch. 2014. *Modeled Distributions of 12 Tree Species in New York*. U.S. Department of Agriculture, Forest Service, Northern Research Station. <https://doi.org/10.2737/nrs-rmap-5>.
- Riemann, Rachel I., Barry Tyler Wilson, Andrew Lister, and Sarah Parks. 2010. “An Effective Assessment Protocol for Continuous Geospatial Datasets of Forest Characteristics Using USFS Forest Inventory and Analysis (FIA) Data.” *Remote Sensing of Environment* 114 (10): 2337–52. <https://doi.org/10.1016/j.rse.2010.05.010>.
- Roy, D. P., V. Kovalsky, H. K. Zhang, E. F. Vermote, L. Yan, S. S. Kumar, and A. Egorov. 2016. “Characterization of Landsat-7 to Landsat-8 Reflective Wavelength and Normalized Difference Vegetation Index Continuity.” *Remote Sensing of Environment* 185 (November): 57–70. <https://doi.org/10.1016/j.rse.2015.12.024>.
- Shi, Yu, Guolin Ke, Damien Soukhavong, James Lamb, Qi Meng, Thomas Finley, Taifeng Wang, et al. 2022. *Lightgbm: Light Gradient Boosting Machine*. <https://github.com/Microsoft/LightGBM>.
- Simard, Marc, Naiara Pinto, Joshua B. Fisher, and Alessandro Baccini. 2011. “Mapping Forest Canopy Height Globally with Spaceborne Lidar.” *Journal of Geophysical Research* 116 (G4). <https://doi.org/10.1029/2011jg001708>.
- Stehman, Stephen V., and Giles M. Foody. 2019. “Key Issues in Rigorous Accuracy Assessment of Land Cover Products.” *Remote Sensing of Environment* 231 (September): 111199. <https://doi.org/10.1016/j.rse.2019.05.018>.
- U.S. Geological Survey. 2019. “3D Elevation Program 1-Meter Resolution Digital Elevation Model.” <https://www.usgs.gov/the-national-map-data-delivery>.
- US Census Bureau. 2013. “TIGER/Line Shapefiles.” <https://www.census.gov/geographies/mapping-files/time-series/geo/tiger-line-file.html>.
- USGS. 2018. “Landsat Collections.” US Geological Survey. <https://doi.org/10.3133/fs20183049>.
- Virginia Tech. 2023a. “Overview of the National Scale Volume and Biomass Estimators (NSVB): State Report for Indiana.” https://charcoal2.cnre.vt.edu/nsvb_factsheets/Reports/State/Indiana.html.
- . 2023b. “Overview of the National Scale Volume and Biomass Estimators (NSVB): State Report for New York.” https://charcoal2.cnre.vt.edu/nsvb_factsheets/Reports/State/New%20York.html.

- . 2023c. “Overview of the National Scale Volume and Biomass Estimators (NSVB): State Report for Washington.” https://charcoal2.cnre.vt.edu/nsvb_factsheets/Reports/State/Washington.html.
- Walker, Kyle. 2023. *tigris: Load Census TIGER/Line Shapefiles*. <https://CRAN.R-project.org/package=tigris>.
- Westfall, James A., John W. Coulston, Andrew N. Gray, John D. Shaw, Philip J. Radtke, David M. Walker, Aaron R. Weiskittel, et al. 2023. *A National-Scale Tree Volume, Biomass, and Carbon Modeling System for the United States*. U.S. Department of Agriculture, Forest Service. <https://doi.org/10.2737/wo-gtr-104>.
- Whitney, Gordon G. 1994. *From Coastal Wilderness to Fruited Plain: A History of Environmental Change in Temperate North America from 1500 to the Present*. Cambridge, United Kingdom: Cambridge University Press.
- Willmott, Cort J., Scott M. Robeson, and Kenji Matsuura. 2011. “A Refined Index of Model Performance.” *International Journal of Climatology* 32 (13): 2088–94. <https://doi.org/10.1002/joc.2419>.
- Wilson, B. Tyler, Andrew J. Lister, and Rachel I. Riemann. 2012. “A Nearest-Neighbor Imputation Approach to Mapping Tree Species over Large Areas Using Forest Inventory Plots and Moderate Resolution Raster Data.” *Forest Ecology and Management* 271 (May): 182–98. <https://doi.org/10.1016/j.foreco.2012.02.002>.
- Wilson, B. Tyler, Andrew J. Lister, Rachel I. Riemann, and Douglas M. Griffith. 2013. “Live Tree Species Basal Area of the Contiguous United States (2000-2009).” *Forest Service Research Data Archive*. Forest Service Research Data Archive. <https://doi.org/10.2737/rds-2013-0013>.
- Wolpert, David H. 1992. “Stacked Generalization.” *Neural Networks* 5 (2): 241–59. [https://doi.org/10.1016/s0893-6080\(05\)80023-1](https://doi.org/10.1016/s0893-6080(05)80023-1).
- Woodall, Christopher W., G. M. Domke, D. W. Macfarlane, and C. M. Oswalt. 2011. “Comparing Field- and Model-Based Standing Dead Tree Carbon Stock Estimates Across Forests of the US.” *Forestry* 85 (1): 125–33. <https://doi.org/10.1093/forestry/cpr065>.
- Woodall, Christopher W., Linda S. Heath, Grant M. Domke, and Michael C. Nichols. 2011. “Methods and Equations for Estimating Aboveground Volume, Biomass, and Carbon for Trees in the u.s. Forest Inventory, 2010.” U.S. Department of Agriculture, Forest Service, Northern Research Station. <https://doi.org/10.2737/nrs-gtr-88>.
- Wright, Marvin N., and Andreas Ziegler. 2017. “**Ranger**: A Fast Implementation of Random Forests for High Dimensional Data in C++ and R.” *Journal of Statistical Software* 77 (1). <https://doi.org/10.18637/jss.v077.i01>.
- Zheng, D, L S Heath, and M J Ducey. 2007. “Forest Biomass Estimated from MODIS and FIA Data in the Lake States: MN, WI and MI, USA.” *Forestry* 80 (3): 265–78. <https://doi.org/10.1093/forestry/cpm015>.
- Zhu, Zhe, and Curtis E Woodcock. 2014. “Continuous Change Detection and Classification of Land Cover Using All Available Landsat Data.” *Remote Sensing of Environment* 144 (March): 152–71. <https://doi.org/10.1016/j.rse.2014.01.011>.